Non-Fullerene Acceptors with an Extended Pi-Conjugated Core: Third Components in Ternary Blends for High-Efficiency, Post Treatment-Free, Organic Solar Cells

Yatzil Alejandra Avalos Quiroz, Olivier Bardagot, Yann Kervella, Cyril Aumaître, Lydia Cabau, Agnès Rivaton, Olivier Margeat, Christine Videlot-Ackermann, Uyxing Vongsaysy, Jörg Ackermann, et al.

FULL PAPER

Non-Fullerene Acceptors with an Extended Pi-Conjugated Core: Third Components in Ternary Blends for High-Efficiency, Post Treatment-Free, Organic Solar Cells

Yatzil Alejandra Avalos-Quiroz,[a] Olivier Bardagot,[b] Yann Kervella,[b] Cyril Aumaître,[b] Lydia Cabau,[b] Agnès Rivaton,[c] Olivier Margeat,[a] Christine Videlot-Ackermann,[a] Uyxing Vongsaysy,[d] Jörg Ackermann,*[a] and Renaud Demadrille.*[b]

[a] Y. A. Avalos-Quiroz, Dr. O. Margeat, Dr. C. Videlot-Ackermann, Dr. J. Ackermann*
Aix Marseille Univ., UMR CNRS 7325, CINaM, 13288 Marseille, France.
E-Mail : ackermann@cinam.univ-mrs.fr
[b] Dr. O. Bardagot, Y. Kervella, Dr. C. Aumaître, Dr. L. Cabau, Dr. R. Demadrille*
University Grenoble Alpes, CEA/CNRS/IRIG, Grenoble, France
E-Mail : renaud.demadrille@cea.fr
[c] Dr. A. Rivaton
Univ. Clermont Auvergne, CNRS, SIGMA Clermont, Inst. de Chimie de Clermont-Ferrand, UMR 6296, F-63000 Clermont-Ferrand, France
[d] Dr. U. Vongsaysy,
ARMOR Solar Power Films SAS, Nantes, France
Supporting information for this article is given via a link at the end of the document.
Twitter : @IRIG_Grenoble @CyrilAumaitre @RDemadrille

Abstract: We report the synthesis of four non-fullerene acceptors (NFAs) with a "A-π-D-π-A" structure, in which the electron-donating core is extended. The molecules are differing by the nature of the solubilizing groups on the π-spacer and/or the presence of fluorine atoms on the peripheral electron-accepting units. The optoelectronic properties of the molecules are characterized in solution, in thin film and in photovoltaic devices. The nature of the solubilizing groups has a minor influence on the optoelectronic properties but affects the organization in the solid state. On the other hand, the fluorine atoms influence the optoelectronics properties and increase the photo-stability of the molecules in thin films. Compare to reference ITIC, the extended molecules show a wider absorption across the visible range and higher LUMO energy levels. The photovoltaic performances of the four NFAs were assessed in binary blends using PM6 (PBDB-T-2F) as the donating polymer and in ternary blends with ITIC-4F. Solar cells (active area 0.27 cm²) show power conversion efficiencies of up to 11.1% when ternary blends are processed from non-halogenated solvents, without any thermal post-treatment nor use of halogenated additives, making this process compatible with industrial requirements.

Introduction

Organic solar cells (OPV) have faced a strong increase of their performances and competitiveness in the last few years. Thanks to the emergence of non-fullerene small molecule acceptors, the development of the ternary blend approach, and the optimization of interface materials they have demonstrated high power conversion efficiency (PCE), semitransparency[1,2] and compliance with large-scale manufacturing processes. Despite reaching efficiencies above 17%,[3–6] the penetration of this technology on the market remains low. To promote the industrial transfer of OPV devices, research efforts are still needed in particular to improve their manufacturing and long-term stability.[7] Therefore, it appears crucial to develop materials and processing more compatible with industrial requirements.[8,9]

The stunning PCE improvements in the last years of bulk-heterojunction solar cells are correlated to NFA molecular engineering and their use in ternary blends.[10–13] Indeed, the novel generations of NFAs offers better complementarity of absorption with polymers[14] and/or extended absorption ranges toward the near-infrared domain,[15,16] thus leading to higher current density (J_{sc}).[17] They can lead to suitable blend morphologies, resulting in remarkable charge transport properties and exciton splitting efficiencies,[18] minimizing energy loss.[19–22]
Today, a large library of building blocks is available to prepare NFAs and their synthetic versatility affords readily tunable optical and electronic properties.[5] For the optimization of the performances in solar cells, it is crucial to develop narrow band gaps NFAs with a broad and intense absorption in the visible range, while paying attention on the position of the LUMO energy level to maximize the open-circuit voltage (V_{oc}). Besides, in order to achieve an optimal morphology for exciton splitting in active layers, the NFAs must be designed so that they form ordered nanoscale domains in blend films in the range of the exciton diffusion length.[23]
Although being crucial, these requirements, are not sufficient for applications. Apart from being efficient in bulk-heterojunctions, these materials should also demonstrate a high thermal stability and photostability for long-term operation. For a transfer to industry, they also have to be soluble and processable from non-halogenated solvents such as *o*-xylene.[24,25]
Keeping in mind these criteria, we propose in this work a molecular design, inspired by ITIC, in which we extended the electron-donating core of the molecule and functionalized it with multiple solubilizing groups. We also synthesized by comparison with ITIC-4F, the fluorinated derivate leading to improved solubility in *o*-xylene compared to ITIC.[25] Hwang and co-workers recently explored a similar molecular design and demonstrated an enhanced absorptivity of the blends and a good processability, thereby achieving solar 54 cm² modules with efficiencies reaching 9.2%.[26]

Owing to the good performances of NFAs based on 4,9-dihydro-s-indaceno[1,2-b:5,6-b']dithiophene (IDT) units and,[5,27] we synthesized a series of four NFAs called BITIC-C8, BITIC-PhC6, BITIC-PhC6F4 and BITIC-C8F4 based on an IDT central core. The IDT was flanked by two 4H-indeno[1,2-b]thiophene units to give an eleven ring central unit. The 4H-indeno[1,2-b]thiophene spacing units were substituted by 4-hexylphenyl groups for BITIC-PhC6 and BITIC-PhC6F4 and *n*-octyl groups for BITIC-C8 and BITIC-C8F4. As peripheral electron-accepting units 2-(3-oxo-2,3-dihydro-1*H*-inden-1-ylidene)malononitrile or its fluorinated analog, 2-(5,6-difluoro-3-oxo-2,3-dihydro-1*H*-inden-1-ylidene)-malonitrile were employed for BITIC-C8, BITIC-PhC6 and for BITIC-PhC6F4, BITIC-C8F4 respectively (Scheme 1).

The influence of the nature of the solubilizing groups and the presence of fluorine atoms on (i) the optoelectronic properties, (ii) the photo-stability, (iii) the blend morphology, and (iv) the photovoltaic performances, was investigated when processed from halogenated or non-halogenated solvents. Various characterization techniques such as UV-Vis spectroscopy, cyclic voltammetry (CV), atomic force microscopy (AFM) and grazing incident wide angle X-ray scattering (GIWAXS) were employed to draw clear structure-properties relationships. We notably demonstrate that the nature of the solubilizing groups borne on the 4H-indeno[1,2-b]thiophene spacers has a minor influence on the optoelectronic properties but affects the organization in thin films and the performances in solar cells. To the opposite, the fluorine atoms borne on the electron-withdrawing units influence the optoelectronics properties, enhance the photo-stability of the molecules in thin films and improve their photovoltaic performances. Moderate PCEs (< 7%) were obtained when the molecules are blended with PM6 (also known as PBDB-T-2F) despite relatively high V_{oc} around 1 V. When we employed the fluorinated derivatives BITIC-PhC6F4 and BITIC-C8F4 in ternary blends comprising PM6 and ITIC-4F as a second electron acceptor compatible with non-halogenated solvents, higher performances were obtained with PCEs over 11%.

Interestingly, PCEs of up to 11.1% were reached with ternary blends processed from non-halogenated solvents, without any thermal or solvent annealing post-treatment, nor use of halogenated additives; a process more compliant with industrial constraints.

Results and Discussion

Design and Synthesis of the NFAs.

The four NFA present exactly the same pi-conjugated backbone. They are constituted by a central 4,4,9,9-tetrakis(4-octylphenyl)-4,9-dihydro-s-indaceno[1,2-b:5,6-b']dithiophene (IDT) unit connected symmetrically to two indenothiophene (IT) units and finally two 3-oxo-2,3-dihydro-1H-inden-1-ylidene) malononitrile moieties that are used as electron-withdrawing peripheral units. Introducing donating spacers bearing solubilizing groups is a strategy aiming at decreasing energy losses in solar cells by rising the LUMO level while facilitating processability compared to ITIC.[28,29] BITIC-C8 and BITIC-PhC6 are analogs, they only differ from the side groups substituting the bridge of the 4*H*-indeno[1,2-b]thiophene units. For the design of BITIC-PhC6, we chose to attach 4-hexyl-phenyl substituents whereas in BITIC-C8 octyl chains were used. Compounds BITIC-PhC6F4 and BITIC-C8F4 are analogs of BITIC-PhC6 and BITIC-C8 respectively but with two fluorine substituents on each 3-oxo-2,3-dihydro-1H-inden-1-ylidene)malononitrile extremities.

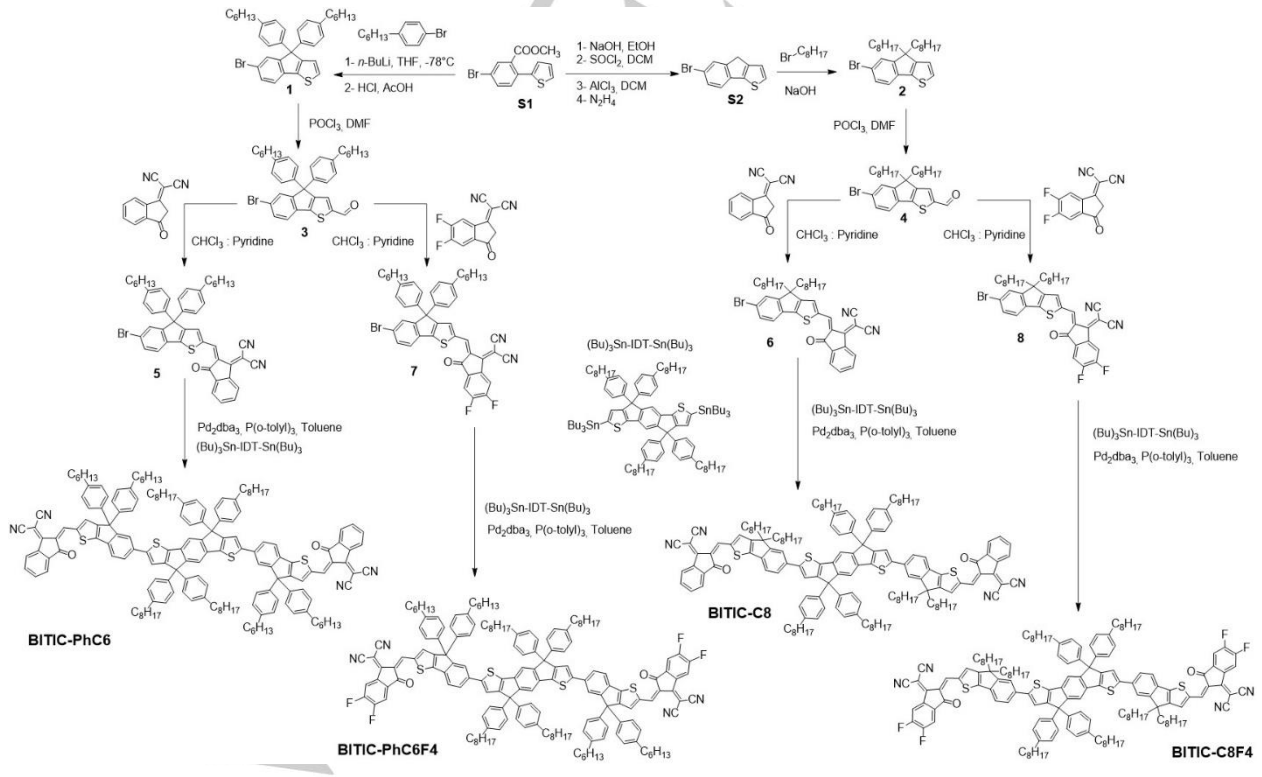

Scheme 1. Synthetic routes and reaction conditions towards the four NFAs (from left to right): BITIC-PhC6, BITIC-PhC6F4, BITIC-C8 and BITIC-C8F4.

The synthesis of the four NFAs is achieved via a convenient convergent synthetic route (see Scheme 1). First, we designed and prepared four different brominated intermediates *i.e.* compounds 5, 6, 7 and 8. These molecules are synthesized in four steps starting from simple precursors S1 and S2. S1 was used to prepare compound 1 whereas S2 was employed to prepare compound 2 according to previously described procedures.[30] Compound 1 and 2 were subsequently formylated under Vilsmeier-Haack conditions to give respectively compound 3 and 4. Then these compounds were condensed through a Knoevenagel reaction to either (3-oxo-2,3-dihydro-1H-inden-1-ylidene)malononitrile or 2-(5,6-difluoro-3-oxo-2,3-dihydro-1*H*-inden-1-ylidene)malononitrile.

In parallel, we prepared the IDT unit, and after stanylation this intermediate was coupled through a Palladium-catalyzed cross-coupling reaction under Stille conditions to the brominated intermediates 5, 6, 7, and 8 to afford the corresponding NFAs BITIC-PhC6, BITIC-C8, BITIC-PhC6F4 and BITIC-C8F4.

Overall, the final compounds are prepared in 7 to 10 steps. They were purified and isolated by silica gel column chromatography and characterized by ^{1}H and ^{13}C nuclear magnetic resonance (NMR) spectroscopy and high-resolution mass spectrometry. The detailed synthesis procedures and the experimental characterization data are provided in the Supplementary Information.

Structure-property relationships, optical properties.

The absorbance spectra of BITIC-C8, BITIC-PhC6, BITIC-PhC6F4 and BITIC-C8F4 recorded in chloroform solution and in thin film are shown in Figure 1. The optical and electrochemical data of the four molecules are collected and compared to the ones of ITIC in Table 1.

In solution, all the NFAs show several absorption bands in the UV-Visible region. Two weak bands appear around 415 nm and 510 nm, whereas the more intense one is located at *circa* 660 nm for BITIC-C8 and BITIC-PhC6 and 680 nm for BITIC-PhC6F4 and BITIC-C8F4. The presence of these two weak bands is a noticeable difference when comparing with ITIC that shows a flatter absorbance spectrum in this range of wavelengths (see ESI). The red shifted absorption observed for BITIC-PhC6F4 and BITIC-C8F4 compared to BITIC-C8 and BITIC-PhC6 suggests a decrease of the band gap originating from the electronegativity of the fluorine atoms. This result is fully consistent with previous studies.[31] Compared to ITIC, the four NFAs show a broader absorption across the visible, with their absorption edges being shifted by *circa* 25 nm for BITIC-C8 and BITIC-PhC6 and 50 nm for BITIC-PhC6F4 and BITIC-C8F4 in solution (see ESI).

The molar absorption coefficients of the new compounds, in the visible, are comprised between 1.5×10^5 and 1.6×10^5 M^{-1} cm^{-1}, which corresponds to an increase of 14% and 18% compared to the one of ITIC found at 1.3×10^5 M^{-1} cm^{-1}.[32]

When the absorbance spectra of the NFAs are measured in thin films casted from chlorobenzene solutions, a red shift is observed for all of them compared to solutions (Table 1). The λ_{max} in the visible range is found at 672 nm and 674 nm for BITIC-PhC6 and BITIC-C8 respectively, and 694 nm and 705 nm for the fluorinated derivatives BITIC-PhC6F4 and BITIC-C8F4. After an annealing treatment of 10 minutes at 120°C no difference in the absorption is observed for BITIC-PhC6 and BITIC-PhC6F4 whereas the films prepared from their analogs BITIC-C8 and BITIC-C8F4 undergo a slight bathochromic shift of 16 nm and 20 nm respectively (Figure 1 and ESI). This result indicates that the introduction of linear alkyl chains on the indeno-thiophene units allows for a reorganization of the molecules upon annealing.

To shed light on the organization of the NFAs in thin films and to understand the effect of the molecular structure and annealing treatment on the reorganization, we investigated the thin films by GIWAXS. We probed the in-plane and out-of-plane orientations for all the NFAs before and after annealing (see ESI).

The in-plane diffraction patterns do not exhibit any noticeable peak for any of the NFAs neither before nor after annealing. This suggests that the films are amorphous in that orientation. However, the out-of-plane diffraction patterns of BITIC-C8 film acquired after annealing at 120°C exhibits two peaks at ~5.3° and 6.6°, attributed to edge-on lamellar packing. The largest lamellar distance found at 16.7 Å is fully consistent with the lamellar distance reported for ITIC, and thus attributed to the interdigitation of the phenyl-hexyl chains on the IDT core. The diffraction patterns of BITIC-C8F4 shows also before and after annealing a larger lamellar distance of 19.4 Å.

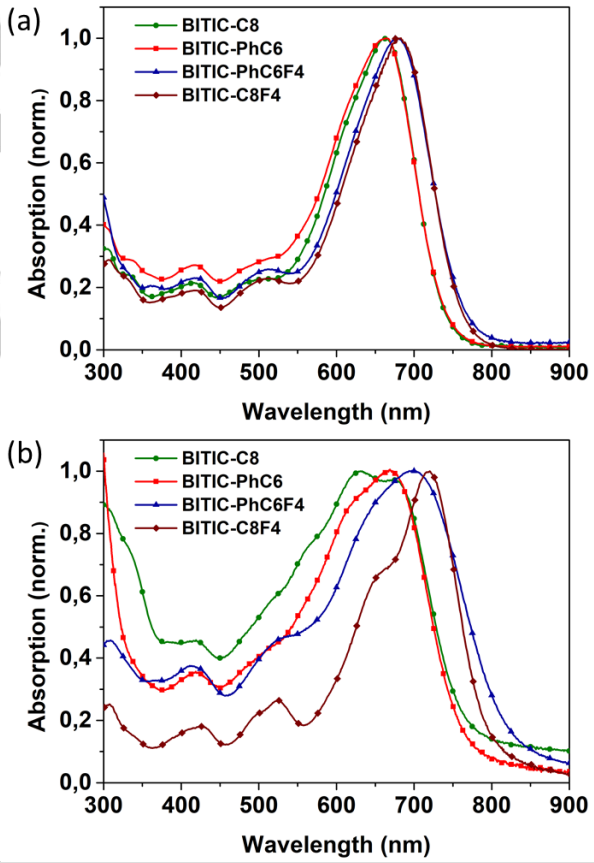

Figure 1: Normalized absorbance spectra of BITIC-C8, BITIC-PhC6, BITIC-PhC6F4 and BITIC-C8F4 (a) in chloroform solutions (concentration 1.10^{-5} M at room temperature) and (b) in thin films casted on glass substrates from chlorobenzene solutions and acquired after thermal annealing at 120° C.

NFAs	λ_{abs} (nm) ε (M^{-1} cm^{-1})[a]	λ_{abs} (nm) Film[b]	λ_{abs} (nm) Film[c]	λ_{edge} (nm) Film[c]	E_{0-0} (eV)	E_{HOMO} (eV)	E_{LUMO} (eV)	$\mu_{electron}$ ($cm^2.V^{-1}.s^{-1}$)
BITIC-C8	662 $1.5x10^5$	674	690	738	1.74	-5.5	-3.8	$3.22x10^{-5}$
BITIC-PhC6	661 $1.5x10^5$	672	672	738	1.57	-5.4	-3.8	$1.00x10^{-5}$
BITIC-PhC6F4	679 $1.6x10^5$	694	694	768	1.39	-5.4	-3.9	$2.85x10^{-5}$
BITIC-C8F4	680 $1.5x10^5$	705	725	766	1.54	-5.5	-3.9	$5.64x10^{-5}$
ITIC	664 $1.3x10^5$	700	714	780	1.58	-5.6	-4.0	$4.50x10^{-3}$

Table 1: Optical and electrochemical data for BITIC-C8, BITIC-PhC6, BITIC-PhC6F4, BITIC-C8F4 and **ITIC.** Data recorded (a) in chloroform solution (concentration 1.10^{-5} M at room temperature) and in thin films casted on glass substrates from chlorobenzene solutions and acquired (b) prior and (c) after thermal annealing at 120°C, during 10 minutes. HOMO and LUMO were calculated from the oxidation potential for the HOMO and reduction potential for the LUMO, measured by CV in dichloromethane solution ($2x\ 10^{-3}$ M) at room temperature, ferrocene/ferrocenium couple was used as the internal standard. Electron mobility determined in organic thin film transistors (OTFTs) configuration (see ESI).

The out-of-plane diffraction patterns acquired for BITIC-PhC6 and BITIC-PhC6F4 do not exhibit any crystalline peaks even after annealing, suggesting that these two NFAs lead to amorphous films, whereas BITIC-C8F4 and BITIC-C8 films show a semi-crystalline nature under these processing conditions. This result is in good agreement with previous studies demonstrating that fluorine atoms induce more non-covalent molecular interactions leading to an improve ordering of the molecules[33] and polymers[34] in the solid state.

Energy levels and DFT calculation

Electrochemical cyclic voltammetry (CV) measurements were carried out in dichloromethane solutions to investigate the redox properties of the molecules and estimate the energy levels of their frontier orbitals (see ESI). The four molecules exhibit a quasi-reversible oxidation wave with onset potentials located between +0.6 V and +0.7 V and a non-reversible reduction wave with onsets positioned between -0.9 and -1.0 V (calibrated by ferrocene-ferrocenium couple, see ESI). Consequently, energy levels are lying between -5.4 and -5.5 eV for the HOMO and between -3.8 and -3.9 eV for the LUMO. Replacing the *n*-octyl chains on the IT units by phenyl-hexyl groups seems to have a minor influence on the frontier orbitals energy levels. Only a slight shift of +0.1 eV is observed for the HOMO. On the other hand, the introduction of two fluorine atoms at both extremities of the molecules slightly shifts towards more negative values (by 0.1 eV) the LUMO level. Such effect of the fluorine substitution was already evidenced in various families of NFAs including ITIC and in polymer series.[35]

Overall, the values deduced from CV experiments are consistent with the ones obtained from DFT calculation (see ESI). Despite a shift of 0.2 to 0.4 eV a similar trend is observed (Figure 2). The optimized molecular structures of the fours NFAs and ITIC and their isoelectronic densities are shown in Figure 2. DFT calculations show that the HOMOs are mainly localized over the IDT donor moieties and their extension is limited to the IT units of the molecules with no overlap with the electron accepting peripheral units. The delocalization of the HOMO is clearly not the same in ITIC where a partial delocalization is found on the two electron-deficient units. On the other hand, the LUMOs of the four molecules are primarily localized on the electron-accepting units with an extension on the indenothiophene spacer units. Here again, this is in contrast with the full delocalization of the LUMO over the core of ITIC, including the IDT central unit.

To conclude this section, the extension of the pi-conjugated core of the molecules with indenothiophene spacer units leads to a better spatial separation of the HOMO-LUMO orbitals. The HOMO is strongly localized on the central IDT unit and consequently it is raises by 0.1-0.2 eV in energy compared to ITIC. The LUMO orbitals are mainly localized on the indenothiophene and the electron-accepting units, hence increasing the LUMO levels by 0.1-0.2 eV. As a result, higher V_{oc} than with ITIC can theoretically be obtained by using these new compounds.

Transport properties

Bottom-gate-bottom-contact (BGBC) organic thin-film transistors (OTFTs) were fabricated to study the transport properties of the extended NFAs. Thin films were processed by spin-coating on top of pre-structured substrates composed of drain and source Au electrodes deposited on SiO_2 dielectric. OTFTs were measured for thin films post-annealed in argon atmosphere (see ESI). Transistor responses, i.e. accumulation mode, were obtained only for positive bias (see ESI) proving that an optimal unipolar electron transport operates in these new NFAs. Maximal electron mobility values are reported in Table 1. Compared to ITIC, a mobility value two orders of magnitude lower is measured for these new NFA compounds. However, the highest electron mobility to $5.64x10^{-5}$ $cm^2.V^{-1}.s^{-1}$ for the fluorinated BITIC-C8F4 compound is consistent with an improve ordering observed in GIWAXS measurements.

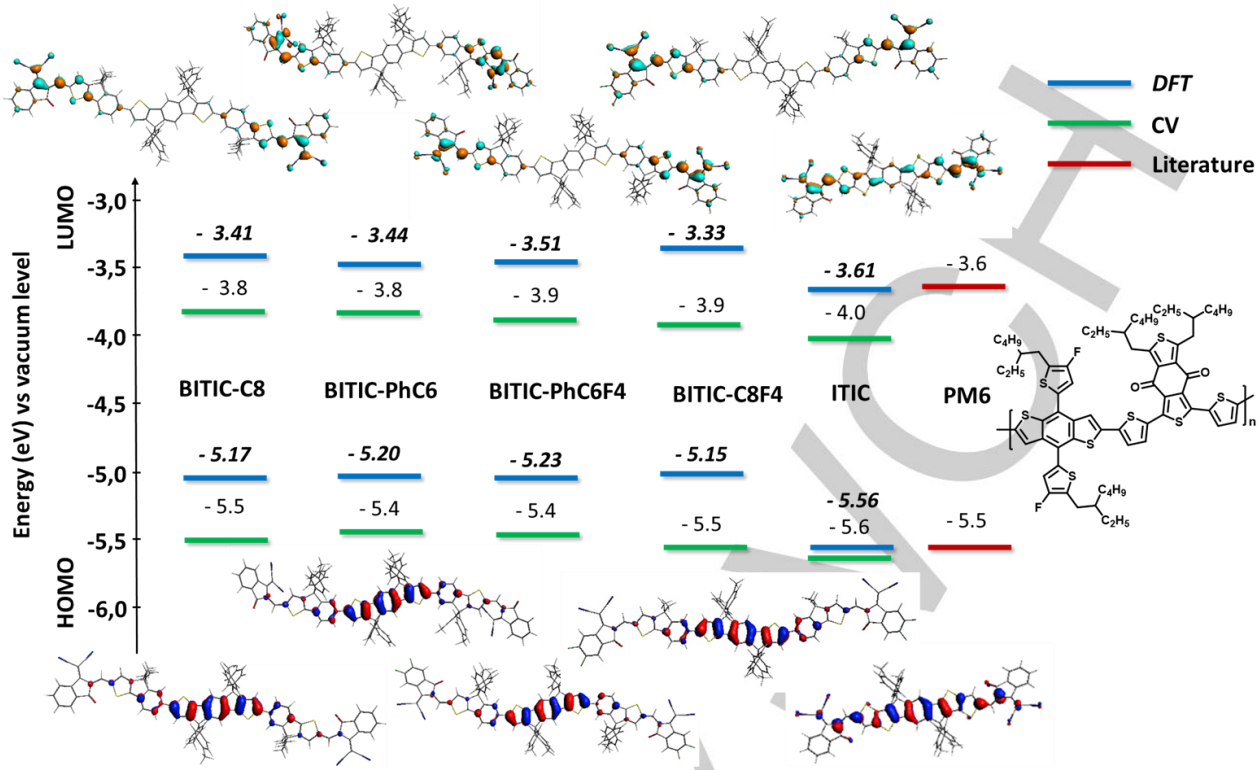

Figure 2: Experimental and DFT calculated energy levels of the frontier orbitals and their spatial localizations for BITIC-C8, BITIC-PhC6, BITIC-PhC6F4, BITIC-C8F4, ITIC and comparison with energy levels of PM6 extracted from literature.[36]

Stability study

In organic photovoltaics, the main research efforts are oriented towards the development of novel materials for gaining higher electrical performances, but very often, the evaluation of their stability is overlooked. To assess the fatigue resistance of the new NFAs, we first subjected the molecules to Thermo-Gravimetric Analysis (TGA). Our measurements show that they are all thermally stable up to around 300°C under Nitrogen and Oxygen atmospheres (see ESI).

Then we evaluated the photostability of the new NFAs. The films casted on glass substrates from chlorobenzene solution were place under inert conditions in a sample holder and sealed in a glass tube under vacuum. Photodegradation experiments were performed in an ageing chamber designed to simulate the AM1.5 spectrum at 1000 W/m^2. UV light below 400 nm was cut off with a UV filter and the temperature of the chamber was set around 35°C. The degradation of the films was monitored by measuring every 100 hours the absorbance spectra of the neat films (see ESI), while the intensity of absorbance at the λ_{max} is plotted in Figure 3 to compare the degradation kinetics of the NFAs. For comparison purpose, ITIC films were investigated under the same conditions. We found that the non-fluorinated molecules BITIC-PhC6 and BITIC-C8 show a rather poor photo-stability as for ITIC losing 40 to 90% of their absorbance after 300 hours of irradiation. However, the fluorinated analogs BITIC-C8F4 and BITIC-PhC6F4 show a better photostability, retaining more than 80% of their absorbance after 300 hours under light-soaking. These results point towards a stabilization effect induced by fluorination, similar as found in solar cells using ITIC derivatives.[37]

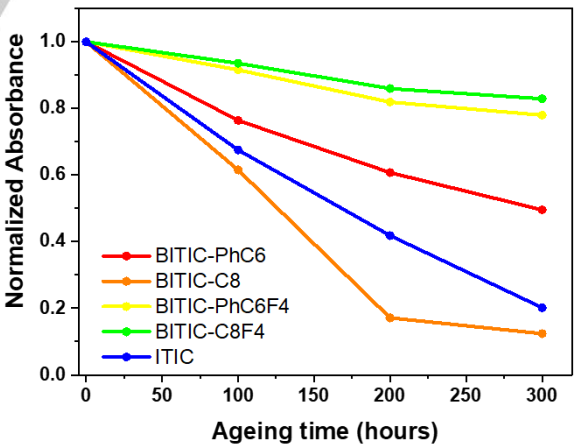

Figure 3: Evolution of the optical density of thin films of BITIC-C8, BITIC-C8F4, BITIC-PhC6, BITIC-PhC6F4, and ITIC, monitored at their respective λ_{max} after ageing under AM1.5 irradiation with a power of irradiation of 1000 W/m^2 at 35°C.

Solar cell properties

Prior to solar cells processing, we first compared the solubility of the extended NFAs in chlorobenzene and *o*-xylene. While all compounds were well dissolved in the chlorinated solvent, only the derivatives BITIC-PhC6F4 and BITIC-C8F4 showed suitable solubility in *o*-xylene. This specificity can be addressed to the presence of fluor atoms, as already found for ITIC-4F.[25]

The photovoltaic properties of the NFAs were thus evaluated by processing BITIC-C8 and BITIC-PhC6 blended with PM6 from chlorobenzene solution while BITIC-PhC6F4 and BITIC-C8F4-based blends were processed from *o*-xylene, identical to PM6:ITIC-4F blend that was used as reference materials.[25]

Prior to device characterization, we studied the surface morphology of the binary blends obtained from the solutions as mentioned before, using Atomic Force Microscopy (AFM). Topography images together with root mean square roughness (rms) are shown in ESI. All blends show similar surface morphology composed of a mixture of fibril and grain-like patterns that are quite typical for blends prepared from PM6.[25] PM6:BITIC-C8, PM6:BITIC-PhC6 and PM6:BITIC-PhC6F4 show rms values of 2.12 nm , 2.03 nm and 2.53 nm, respectively, that are close to PM6:ITIC-4F layers.[25] In contrast, PM6:BITIC-C8F4 blend show a smoother surface with a rms = 0.54 nm. Solar cells using inverted device structures as glass/ITO/ZnO/Active-Layer/MoO_3/Ag were then processed by deposition of the blend solutions on a ZnO electron-transport layer via spin coating under Argon (more details about fabrication in Experimental section). Previous works of ITIC-based solar cells reported an improved device efficiency through enhanced NFA ordering obtained by thermal annealing of the active layer.[38] As the semi-crystalline nature of BITIC-C8 and BITIC-C8F4 described above may be improved by thermal treatments, we thermally annealed the active layers at 120°C and 140°C respectively. The J-V curves of optimized organic solar cells (OSCs) are displayed in Figures 4 and in ESI, with the photovoltaic parameters in Table 2. Compared to ITIC-4F, all compounds lead to solar cells with strongly increased V_{oc} between 0.98 V to 1.1 V due to their larger band gap and higher LUMO level. The fluorinated compounds, BITIC-PhC6F4 and BITIC-C8F4, show the highest efficiencies of 6.73 % and 6.81%, respectively, that is however, clearly below the performance of ITIC-4F-based reference OSC with 11.2%. The performance drop are related to losses in J_{sc} that can be attributed to the lower absorption of the polymer blends based on the new compounds in the 650-750 nm range (see ESI), together with lower fill factor (FF) that can be correlated to the lower electron mobility compared to ITIC-4F as determined before. This is in agreement with the lower external quantum efficiency (EQE) of the fluorinated compounds over the whole absorption spectrum compared to ITIC-4F based solar cells (see ESI). Taking into account the high V_{oc} of OSCs processed with BITIC-C8F4 and BITIC-PhC6F4 together with their high solubility in *o*-xylene, we additionally studied the use of both molecules as a third component in PM6:ITIC-4F based solar cells with the aim to enhance the V_{oc} and thus the efficiency compared to the binary system.

Indeed, the PM6:ITIC-4F:NFA ternary blends present a significantly higher V_{oc} with 0.90 V and 0.91 V, instead of 0.86 V resulting in a PCE of 11.10% for both ternary OSCs with a ratio 1:0.75:0.25 (Table 2). Although a slightly lower J_{sc} is observed in ternary OSCs, the increased V_{oc} preserves the overall efficiency.

The use of a third component helps to obtain continuously tuneable V_{oc} of ternary solar cells; this has been confirmed experimentally by several studies.[39,40]

In conventional binary solar cells, it is generally recognized that the V_{oc} of the binary solar cell is mainly determined by the difference between the HOMO energy level of the donor and the LUMO. The V_{oc} of ternary solar cells is not limited to the smaller V_{oc} value; it can be adjusted depending on the composition of the active layer between the V_{oc} values of the corresponding binary blends solar cells without significant effect on the Jsc or FF. The tuneable V_{oc} in the ternary solar cells was commonly interpreted by the more favourable ratios of charge generation to charge recombination.[41] The increase in V_{oc} is observed in a linear proportion to the amount of BITIC-C8F4 or BITIC-PhC6F4 in the ternary blends (see ESI) suggesting either a parallel-like operating mode or electronic alloy. [41]

AFM images of a ternary film with 25% of BITIC-C8F4 as third component (see ESI) show a surface morphology and a surface roughness similar to the ones of binary PM6:ITIC-4F blends.[25] This result confirms a good miscibility of the new acceptors with ITIC-4F since the ternary blend morphology is comparable to the ITIC-4F based binary blends.[42]

Importantly, we observed that both ternary blends allow to process high efficiency OSC without the use of any thermal annealing, while the binary blend demands for 100°C to reach the same efficiency. Indeed both ternary OSCs using as-casted blend show efficiencies of 11.1% compared to PM6:ITIC-4F with only 10.17% for binary PM6-ITIC-4F OSC as given in Table 2.

The addition of BITIC-PhC6F4 or BITIC-C8F4 as third component therefore offers ternary blends processed from non-halogenated solvents leading to high efficiency, without any thermal treatment, nor use of halogenated additives that clearly improves the compatibility of OSCs for industrial applications.

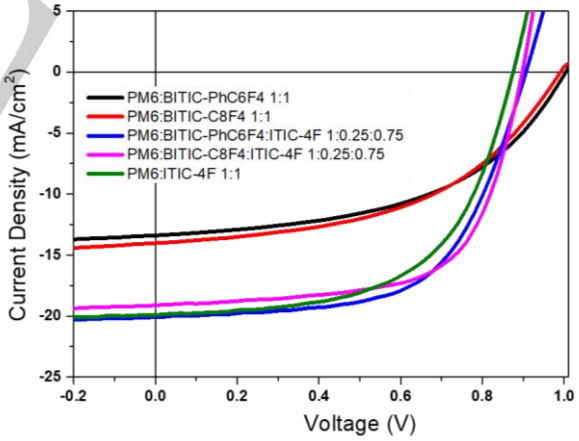

Figure 4: J-V curves of the best solar cells for the binary and ternary blends

Blends Polymer	NFAs	Solvent	Ratio	V_{oc} (V)	J_{sc} (mA/cm^2)	FF (%)	PCE (%)	Treatment
PM6	**BITIC-C8**	Chlorobenzene	1:1	1.08	7.14	45.19	3.48 (3.31 ±0.16)	120°C
PM6	**BITIC-PhC6**	Chlorobenzene	1:1	1.10	5.44	41.17	2.46 (2.42 ±0.04)	120°C
PM6	**BITIC-PhC6F4**	O-Xylene	1:1	0.98	13.12	51.92	6.73 (6.53 ±0.20)	140°C
PM6	**BITIC-C8F4**	O-Xylene	1:1	1.00	14.01	48.59	6.81 (6.60 ±0.20)	140°C
PM6	**ITIC-4F**	O-Xylene	1:1	0.86	20.21	58.31	10.17 (10.14 ±0.03)	As-cast
PM6	**ITIC-4F**	O-Xylene	1:1	0.88	20.97	62.14	11.20 (10.95 ±0.25)	100°C
PM6	**ITIC-4F:BITIC-PhC6F4**	O-Xylene	1:0.75:0.25	0.91	20.09	63.25	11.10 (10.87 ±0.22)	As-cast
PM6	**ITIC-4F:BITIC-C8F4**	O-Xylene	1:0.75:0.25	0.90	19.21	64.51	11.10 (10.74 ±0.40)	As-cast

Table 2: Solar cells fabricated according to an inverted device structure (glass/ITO/ZnO/Active-Layer/MoO_3/Ag), active area 0.27 cm², composition of the active layer and processing conditions, the photovoltaic parameters reported correspond to the best solar cells obtained under the optimized fabrication conditions. In parenthesis, mean values and standard deviation for the PCE obtained from at least three devices.

Conclusion

In conclusion, we designed and synthesized four new NFAs based on an extended pi-conjugated core comprising eleven aromatic rings coded as BITIC-C8, BITIC-PhC6, BITIC-PhC6F4 and BITIC-C8F4. The molecules showed a higher and broader absorption compared to ITIC. Their energy levels were found close to the ones of ITIC, lying between -5.4 eV and -5.5 eV for the HOMOs and -3.8 eV and -3.9 eV for the LUMOs. Surprisingly, the solubility of the molecules in non-halogenated solvents as *o*-xylene is mainly improved by the presence of the fluor atoms rather than the nature of the solubilizing groups. Interestingly, all the molecules showed a high photochemical stability compared to ITIC and a good resistance to thermal oxidation, making them good candidates for the fabrication of solar cells under ambient conditions. OSCs with an area of 0.27 cm² were fabricated and the photovoltaic properties of the extended NFAs were evaluated by blending them with PM6. All compounds lead to solar cells with an increased Voc between 0.98 V and 1.10 V originating from a larger band gap and a higher LUMO level. The fluorinated compounds, BITIC-PhC6F4 and BITIC-C8F4, show the highest efficiencies of 6.73 % and 6.81 % in binary blends. When used as third component together with PM6 and ITIC-4F in a ternary blend, V_{oc} of around 0.90 V, and PCE of 11.1 % are achieved for both NFAs.

We demonstrate in this work that fluorinated NFAs with an extended pi-conjugated core can be advantageously used as third components in ternary blends for the fabrication of high-efficiency, post treatment-free OSCs, representing a step forward future industrial application.

Experimental section

Materials. All polymers and solvents used were commercially available. PBDB-T-2F (PM6) was purchased from 1-materials. *o*-xylene and chlorobenzene were acquired from Sigma Aldrich, while ZnO 2.5% solution was obtained from AVANTAMA.

Film preparation and photodegradation measurements. To prepare neat materials solutions, 10 mg/ml of donor polymer (PM6) and 20 mg/ml of acceptors were dissolved in chlorobenzene (for BITIC-C8 and BITIC-PhC6) or in *o*-xylene (for BITIC-PhC6F4 and BITIC-C8F4) and stirred overnight at 60°C. For stability test, the neat solutions (described below) are then spin-coated on top of cleaned glass and KBr substrates that are subsequently annealed at 100°C for 10 min to eliminate solvent. Then all the films were place under inert conditions in a sample holder and in a glass tube under vacuum. Photodegradation experiments were performed in a SUNTEST CPS/XLS Atlas device designed to simulate the AM1.5 spectrum. UV light below 400 nm were cut off with an industrial UV filter. The black standard temperature was set at 60°C, which corresponds to a chamber temperature of around 35°C. Irradiation provided by a xenon lamp from Atlas (NXE1700) was set at 1000 W/m^2 in the UV–visible domain. UV–visible spectra were obtained on a Shimadzu UV-2600 spectrophotometer equipped with an integrating sphere. The absorbance of the samples was measured and integrated in the 200-1000 nm range. Infrared transmission spectra were recorded with a Thermo Scientific Nicolet 6700 spectrophotometer purged with dry air (32 acquisitions summation with 4 cm^{-1} resolution). The sample holder used for the films allowed measuring the same spot in the film.

Solar cells fabrication and I-V measurement. PM6:BITIC-C8 and PM6:BITIC-PhC6 inks were prepared in chlorobenzene in a total concentration of 24 mg/ml in different weight ratios and stirred at 60°C overnight. PM6:BITIC-PhC6F4, PM6:BITIC-C8F4 and PM6:ITIC-4F inks were prepared in *o*-xylene at 20 mg/ml total concentration with a 3.5%v/v of tetraline at room temperature. The ternary blends PM6:ITIC-4F:BITIC-PhC6F4 and PM6:ITIC-4F:BITIC-C8F4 were mixed in *o*-xylene with a 3.5%v/v tetraline in different BITIC-PhC6F4 and BITIC-C8F4 ratios (25%, 50% and 75%) at room temperature. ITO-coated glass (sheet resistance 10-15 Ω/) purchased from LUMTEC were sequentially cleaned with deionized water, acetone and isopropanol under sonication for 15 min each, dried with argon and then treated in a UV-ozone oven for 15 min at 80°C. All the devices were fabricated in inverted structure ITO/ZnO/Active Layer/MoO_3/Ag. ZnO layer was spin-coated in air from a 1% v/v solution in isopropanol at 5000 rpm follow by thermal annealing at 120°C for 10 min. The substrates were then transferred to a N_2-filled glovebox where a blend film of 90-100 nm thickness was spin-coated on top of ZnO films. At this stage of solar cell fabrication, a thermal annealing was applied at 100-140°C for 10 min. Finally, 5 nm MoO_3 and 100 nm Ag were deposited by thermal evaporation thought a mask to define an active area of 0.27 cm^2. The current density-voltage characterization of the devices under AM1.5G light solar simulator (Newport Sol3A Class AAA) were recorded with a Keithley 238 source meter unit inside the glove box. The illumination

intensity of the light source was calibrated to be 100 mW/cm^2 using a standard silicon solar cell (Newport Company, Oriel no. 94043A) calibrated by the National Renewable Energy Laboratory (NREL). The EQE of the solar cells was measured using a 150 W Xenon arc lamp along with Oriel Cornerstone 260 monochromator.

Thin film transistor fabrication and characterization. Interdigitated TFT structures were purchased from Fraunhofer (Germany) with n-doped silicon wafers covered with thermally grown silicon dioxide (SiO_2) followed by a lift-off deposited source and drain electrodes composed of 10 nm of indium tin oxide (ITO) and 30 nm of gold (Au). Channel length L to channel width W ratios were 20/10000 µm or 10/10000 µm. Prior the deposition of the NFA-based solutions by spin-coating, the substrates were first cleaned. The both electrodes and SiO_2 dielectric surfaces were chemically modified with a thiol derivative, namely 4-(dimethylamino) benzenethiol (DABT) and divinyl-tetramethyldisiloxane-bis(benzocyclobutene (BCB), respectively.[43,44] NFAs solutions were prepared in chlorobenzene (for BITIC-C8 and BITIC-PhC6) or *o*-xylene (for BITIC-PhC6F4 and BITIC-C8F4) at a concentration of 10 mg/ml and stirred overnight at 60°C for chlorobenzene and room temperature for *o*-xylene. Solutions were spin-coated at 1000 rpm with a spin-coater machine from SET Company (model TP 6000) on top of the source and drain electrodes. OTFTs thus produced were annealed on a preheated hot plate at 120°C (for BITIC-C8 and BITIC-PhC6) or 140°C (for BITIC-PhC6F4 and BITIC-C8F4) for 10 min. Current-voltage characteristics were performed with a Hewlett-Packard 4140B pico-amperemeter-DC voltage source. The mobility values µ were extracted from the saturation region of the transfer curves with the equation: $I_D = W/2L\, C_{ox}\mu\, (V_G - V_T)^2$ where I_D is the drain-source voltage, C_{ox} is the capacitance per unit area of the gate insulator layer (C_{ox} = 18.8×10^{-9} F.cm^{-2}), V_G is the gate voltage, V_T is the threshold voltage, and µ is the field-effect mobility. All electrical characterization results were performed in nitrogen-filled glove box.

Thin film characterization Surface morphology of NFAs-based blends was investigated by either (i) atomic force microscopy (AFM NTEGRA from NT-MIDT) in tapping mode by using the silicon tips (MikroMash) with theoretical resonant frequency of 300 kHz and a spring constant of 16 N m^{-1} at room temperature or (ii) in peak-force mode under ambient conditions, using a Bruker Dimension-Icon AFM (ScanAsyst-Air cantilevers, stiffness 0.4 N/m). GIWAXS experiments were recorded with thin film on glass substrates under ambient atmosphere using a laboratory Rigaku Smartlab diffractometer (Cu, $\lambda_{K\alpha}$ = 1.54184 Å, 8 kV).

Contributions

LC synthesized the intermediate molecules and YK synthesized the NFA. OB and CA performed the optoelectronic characterizations and the theoretical modelling of the NFA compounds. YAAQ, OM and CVA developed, fabricated and characterized the OSCs and the OTFTs and optimized the devices. AR and YAAQ performed the photodegradation study. UV contributed in the optimization of the deposition process. JA and RD designed the experiments and the molecules, supervised the work, analysed the data and wrote the manuscript. All the authors contributed to the analysis of the data and the preparation of the manuscript and ESI.

Acknowledgements

This project has received funding by the French Research Agency (project ANR-17-CE05-0020-01 named NFA-15) and the LABEX Laboratoire d'Alliances Nanosciences-Energies du Futur (LANEF, ANR-10-LABX-51-01). A. A. Medjahed and S. Pouget are acknowledged for their help in the GIWAXS measurements. Dr. P. Maldivi is acknowledged for training OB and for her assistance in the modelling study of the compounds. M. Bertrand is acknowledged for helpful discussions on the results and the fabrication of the devices.

Keywords: NFA • Bulk-heterojunction • Organic photovoltaics • Organic solar cells • Ternary blend •

Entry for the Table of Contents

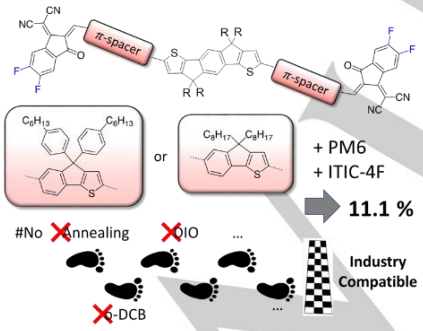

Four non-fullerene acceptors with an extended pi-conjugated core are synthesized and their optoelectronic properties are fully described. The fluorinated NFAs are soluble in non-halogenated solvents and demonstrate a high photochemical stability. We show that they can be advantageously used as third components in ternary blends with PM6 and ITIC-4F for the fabrication of high-efficiency, post treatment-free organic solar cells.

References

[1] Y. Bai, C. Zhao, X. Chen, S. Zhang, S. Zhang, T. Hayat, A. Alsaedi, Z. Tan, J. Hou, Y. Li, *J. Mater. Chem. A* **2019**, *7*, 15887–15894.

[2] V. V. Brus, J. Lee, B. Luginbuhl, S. Ko, G. C. Bazan, T. Nguyen, *Adv. Mater.* **2019**, *31*, 1900904.

[3] D. Zhou, W. You, H. Xu, Y. Tong, B. Hu, Y. Xie, L. Chen, *J. Mater. Chem. A* **2020**, *8*, 23096–23122.

[4] Y. Cui, H. Yao, J. Zhang, K. Xian, T. Zhang, L. Hong, Y. Wang, Y. Xu, K. Ma, C. An, C. He, Z. Wei, F. Gao, J. Hou, *Adv. Mater.* **2020**, *32*, 1908205.

[5] F. Zhao, H. Zhang, R. Zhang, J. Yuan, D. He, Y. Zou, F. Gao, *Adv. Energy Mater.* **2020**, *10*, 2002746.

[6] C. Li, J. Zhou, J. Song, J. Xu, H. Zhang, X. Zhang, J. Guo, L. Zhu, D. Wei, G. Han, J. Min, Y. Zhang, Z. Xie, Y. Yi, H. Yan, F. Gao, F. Liu, Y. Sun, *Nat. Energy* **2021**, DOI 10.1038/s41560-021-00820-x.

[7] Q. Zhao, Z. Xiao, J. Qu, L. Liu, H. Richter, W. Chen, L. Han, M. Wang, J. Zheng, Z. Xie, L. Ding, F. He, *ACS Energy Lett.* **2019**, *4*, 1106–1114.

[8] R. Szymanski, R. Henry, S. Stuard, U. Vongsaysy, S. Courtel, L. Vellutini, M. Bertrand, H. Ade, S. Chambon, G. Wantz, *Sol. RRL* **2020**, *4*, 2000538.

[9] M. Mainville, M. Leclerc, *ACS Energy Lett.* **2020**, *5*, 1186–1197.

[10] A. Wadsworth, M. Moser, A. Marks, M. S. Little, N. Gasparini, C. J. Brabec, D. Baran, I. McCulloch, *Chem. Soc. Rev.* **2019**, *48*, 1596–1625.

[11] Z. Peng, K. Jiang, Y. Qin, M. Li, N. Balar, B. T. O'Connor, H. Ade, L. Ye, Y. Geng, *Adv. Energy Mater.* **2021**, *11*, 2003506.

[12] K. Zhang, J. Guo, L. Zhang, C. Qin, H. Yin, X. Gao, X. Hao, *Adv. Funct. Mater.* **2021**, *31*, 2100316.

[13] B.-H. Jiang, C.-P. Chen, H.-T. Liang, R.-J. Jeng, W.-C. Chien, Y.-Y. Yu, *Dye. Pigment.* **2020**, *181*, 108613.

[14] K. He, P. Kumar, Y. Yuan, Y. Li, *Mater. Adv.* **2021**, *2*, 115–145.

[15] J. Zhao, C. Yao, M. U. Ali, J. Miao, H. Meng, *Mater. Chem. Front.* **2020**, *4*, 3487–3504.

[16] S. Pang, X. Zhou, S. Zhang, H. Tang, S. Dhakal, X. Gu, C. Duan, F. Huang, Y. Cao, *ACS Appl. Mater. Interfaces* **2020**, *12*, 16531–16540.

[17] A. A. Mohapatra, V. Tiwari, S. Patil, *Energy Environ. Sci.* **2021**, *14*, 302–319.

[18] N. Gasparini, A. Wadsworth, M. Moser, D. Baran, I. McCulloch, C. J. Brabec, *Adv. Energy Mater.* **2018**, *8*, 1703298.

[19] P. Cheng, G. Li, X. Zhan, Y. Yang, *Nat. Photonics* **2018**, *12*, 131–142.

[20] X. He, L. Yin, Y. Li, *J. Mater. Chem. C* **2019**, *7*, 2487–2521.

[21] X. Xu, K. Feng, Y. W. Lee, H. Y. Woo, G. Zhang, Q. Peng, *Adv. Funct. Mater.* **2020**, *30*, 1907570.

[22] A. Karki, J. Vollbrecht, A. J. Gillett, P. Selter, J. Lee, Z. Peng, N. Schopp, A. L. Dixon, M. Schrock, V. Nádaždy, F. Schauer, H. Ade, B. F. Chmelka, G. C. Bazan, R. H. Friend, T. Nguyen, *Adv. Energy Mater.* **2020**, *10*, 2001203.

[23] T. Shan, K. Ding, L. Yu, X. Wang, Y. Zhang, X. Zheng, C. Chen, Q. Peng, H. Zhong, *Adv. Funct. Mater.* **2021**, 2100750.

[24] S. H. Park, N. Y. Kwon, H. J. Kim, E. Cho, H. Kang, A. K. Harit, H. Y. Woo, H. J. Yoon, M. J. Cho, D. H. Choi, *ACS Appl. Mater. Interfaces* **2021**, *13*, 13487–13498.

[25] P. Perkhun, W. Köntges, F. Pourcin, D. Esteoulle, E. Barulina, N. Yoshimoto, P. Pierron, O. Margeat, C. Videlot-Ackermann, A. K. Bharwal, D. Duché, C. R. Herrero, C. Gonzales, A. Guerrero, J. Bisquert, R. R. Schröder, M. Pfannmöller, S. Ben Dkhil, J. Simon, J. Ackermann, *Adv. Energy Sustain. Res.* **2021**, *2*, 2000086.

[26] H. S. Kim, S. Rasool, W. S. Shin, C. E. Song, D.-H. Hwang, *ACS Appl. Mater. Interfaces* **2020**, *12*, 50638–50647.

[27] M. H. Elsayed, B.-H. Jiang, Y.-P. Wang, P.-Y. Chang, Y.-C. Chiu, R.-J. Jeng, H.-H. Chou, C.-P. Chen, *J. Mater. Chem. A* **2021**, *9*, 9780–9790.

[28] Z. Kang, Y. Ma, Q. Zheng, *Dye. Pigment.* **2019**, *170*, 107555.

[29] C. H. Jeong, Y. U. Kim, C. G. Park, S. Choi, M. J. Cho, D. H. Choi, *Synth. Met.* **2018**, *246*, 164–171.

[30] D. Joly, L. Pellejà, S. Narbey, F. Oswald, T. Meyer, Y. Kervella, P. Maldivi, J. N. Clifford, E. Palomares, R. Demadrille, *Energy Environ. Sci.* **2015**, *8*, 2010–2018.

[31] T. J. Aldrich, M. Matta, W. Zhu, S. M. Swick, C. L. Stern, G. C. Schatz, A. Facchetti, F. S. Melkonyan, T. J. Marks, *J. Am. Chem. Soc.* **2019**, *141*, 3274–3287.

[32] Y. Lin, J. Wang, Z.-G. Zhang, H. Bai, Y. Li, D. Zhu, X. Zhan, *Adv. Mater.* **2015**, *27*, 1170–1174.

[33] S. Dai, J. Zhou, S. Chandrabose, Y. Shi, G. Han, K. Chen, J. Xin, K. Liu, Z. Chen, Z. Xie, W. Ma, Y. Yi, L. Jiang, J. M. Hodgkiss, X. Zhan, *Adv. Mater.* **2020**, *32*, 2000645.

[34] B. Li, Q. Zhang, G. Dai, H. Fan, X. Yuan, Y. Xu, B. Cohen-Kleinstein, J. Yuan, W. Ma, *J. Mater. Chem. C* **2019**, *7*, 12641–12649.

[35] T. Olla, O. A. Ibraikulov, S. Ferry, O. Boyron, S. Méry, B. Heinrich, T. Heiser, P. Lévêque, N. Leclerc, *Macromolecules* **2019**, *52*, 8006–8016.

[36] J. Wu, Y. Meng, X. Guo, L. Zhu, F. Liu, M. Zhang, *J. Mater. Chem. A* **2019**, *7*, 16190–16196.

[37] X. Du, T. Heumueller, W. Gruber, A. Classen, T. Unruh, N. Li, C. J. Brabec, *Joule* **2019**, *3*, 215–226.

[38] Q. Liang, J. Han, C. Song, X. Yu, D.-M. Smilgies, K. Zhao, J. Liu, Y. Han, *J. Mater. Chem. A* **2018**, *6*, 15610–15620.

[39] Q. S. An, F. J. Zhang, L. L. Li, J. Wang, Q. Q. Sun, J. Zhang, W. H. Tang and Z. B. Deng, *ACS Appl. Mater. Interfaces*, **2015**, *7*, 3691–3698.

[40] B. M. Savoie, S. Dunaisky, T. J. Marks and M. A. Ratner, *Adv. Energy Mater*., **2015**, *5*, 1400891.

[41] Q. An, F. Zhang, J. Zhang, W. Tang, Z. Deng, B. Hu, *Energy Environ. Sci.* **2016**, *9*, 281-322

[42] R. Yu, S. Zhang, H. Yao, B. Guo, S. Li, H. Zhang, M. Zhang, J. Hou, *Adv. Mater*. **2017**, 29, 1700437.

[43] M. Robin, M. Harnois, Y. Molard, E. Jacques, *Org. Electron.* **2016**, *39*, 214-221

[44] Y. Park, C. Fuentes-Hernandez, X. Jia, F. A. Larrain, J. Zhang, S. R. Marder, B. Kippelen. *Org. Electron*. **2018**, *58*, 290–293.